Journal of Hydroscience and Hydraulic Engineering
Vol. 7, No. 1, November, 1989, pp.51-62

THREE-DIMENSIONAL CALCULATION OF FLOW IN RIVER CONFLUENCES USING BOUNDARY-FITTED COORDINATES

By

S.B. Weerakoon, Graduate Student

and

Nobuyuki Tamai, Professor

Dept. of Civil Engineering, Univ. of Tokyo, Tokyo 113, Japan.

SYNOPSIS

A three-dimensional mathematical model, based on finite volume method and $k-\epsilon$ turbulence model, for predicting steady state confluence flow without recirculation is presented. The model covers the confluence region by a curvilinear grid which is generated numerically using a quasiconformal mapping method. The water body in the confluence region is thus transformed to a parallelepiped and the computation is done in the transformed domain. The model performance is first verified by applying it to compute flow in a parallel flow confluence where comparison of the results with experimental results is shown to be satisfactory. Then, the model is employed to predict the flow in a confluence of 60 degrees with a training levee. The prediction agrees well with the experimental results. The performance of a levee which facilitates two streams to mix gradually and thereby to reduce the superelevation and the secondary flow in the main stream, is demonstrated.

INTRODUCTION

The confluences, where the tributaries join with the main streams are common in river systems and therefore the understanding of the mechanism governing the flow and the flow field itself in a confluence is important in both flood control and water utilization. However, flow situation in a natural river confluence is very complex in three dimensions not only due to the coexistance of mixing, secondary flow and flow separation but also due to the irregular topography subjected to continuous change by erosion, silting and sediment transport processes. Despite these barriers caused the confluences not to be well tackled yet by the researchers, enormous experience of hydraulic engineers has permited to adopt some measures such as construction of training levees to control the flow in river confluences.

Among the limited literature available, Taylor(23), Webber and Greated(25) and Ramamurthy et. al(18) have reported relations between the depth of flow at the confluence region and the discharge ratio on the basis of conservations of momentum and energy. Webber and Greated(25), Modi et al.(14) and Fujita and Komura(6) have reported theoritical solutions for confluence flow by method of conformal mapping and predicted the recirculation zone and streamline pattern. However, the theoritical procedures needed oversimplifications including the assumption of inviscid two-dimensional flow despite the strongly three-dimensional nature of the flow. As for experimental studies, Best and Reid(3) observed the increase in size of the recirculation zone with the increase of confluence angle and with the increase of discharge ratio by visualization method. Koike(9) studied a parallel flow confluence and reported detail measurements of velocity profiles, turbulence quantities and large eddies in the developing mixing layer. Tada(21) carried out series of experiments to study the role of a levee in a confluence and his measurements shows the shift of maximum velocity below the water surface due to the secondary flow. Fujita and Komura(7) observed the recirculation zone and bed-shear stress direction for a confluence of 90 degrees. They also reported the measurements of secondary flow in selected sections. Mosely(15) , Ashmore and Parker(1) studied the scour hole in confluences with erodible bed. They found two secondary flow cells rotate in opposite directions and their role in local scour. Best(2) observed the sediment transport process and its effect on the local scour. From above three separate studies on erodible bed it can be learnt that confluence angle,

discharge ratio, Froude number and bed material are the main parameters to govern the flow in a confluence.

As the theoritical and experimental approaches have their limitations, numerical simulation becomes an important tool. Tamai and Ueda(22) developed a three-dimensional numerical model based on the $k-\epsilon$ turbulence model and partially parabolic solution procedure for the confluence of 30 degrees with no recirculation. The model predicts the mixing of two flows and the two counter rotating secondary flow cells. However the model is applicable only for the small confluence angles due to the restraints in the grid system adopted. Present paper describes a three-dimensional mathematical model which employs a numerical grid generation technique and hence capable of tackling an arbitrary confluence geometry. Similar to the previous model, some idealizations are made for a natural confluence to arrive computationally tactable configuration. The channel bed and banks are assumed to be nominally smooth and stable, and the flow is assumed to be symmetric about the top surface. The model is based on the finite difference solution of the time-averaged Navier-Stokes equations, continuity equation and the standard $k-\epsilon$ model. The streamwise diffusion is neglected in the model as partially parabolic flow computation procedure is adopted. The model is therefore restricted to confluence flows with no recirculation. This paper presents details of the model and its predictions for two different confluence flows.

GRID GENERATION

Boundary-fitted curvilinear coordinates are used in the present work since it has some advantages over the Cartesian coordinates in the confluence flow computations. For example, application of boundary conditions is simple, numerically accurate as the deviation of grid lines from streamlines is small and the grids can be distributed so as to have fine grids at the regions of high gradients while maintaining the uniform square meshes in the computational domain.

A quasiconformal mapping method which enables to distribute coordinate lines at the required spacings is employed to generate a smooth and nearly-orthogonal curvilinear grid. The present method is simpler than the methods given in Thompson and Warsi(24), Mastin and Thompson(12), Chen et al.(4) for river flow computations. The grid generation in three-dimensional domain comprises of first the generation in two-dimensional flat surface and then the extension to the third dimension.

If y^1, y^2 and x^1, x^2 are the Cartesian and curvilinear coordinates respectively, then

$$\vec{g_r} = \frac{\partial y^m}{\partial x^r}\vec{\imath_m} \tag{1}$$

$$\vec{g_r}.\vec{g_s} = g_{rs} \tag{2}$$

where $\vec{\imath_m}$ = the unit vector in Cartesian coordinates; $\vec{g_r}$ = base vector in curvilinear coordinates; and g_{rs} = metric tensor. From eqn. 2, following orthogonal mapping relation can be derived.

$$\frac{\partial y^2}{\partial x^1} = D(\frac{\partial y^1}{\partial x^2}) \tag{3}$$

$$\frac{\partial y^1}{\partial x^1} = -D(\frac{\partial y^2}{\partial x^2}) \tag{4}$$

where $D = \sqrt{g_{11}/g_{22}}$ = the grid aspect ratio. Combining eqns. 3 and 4 following elliptic system of equations in the transformed domain can be obtained.

$$\frac{\partial}{\partial x^1}(\frac{1}{D}\frac{\partial y^1}{\partial x^1}) + \frac{\partial}{\partial x^2}(D\frac{\partial y^1}{\partial x^2}) = 0 \tag{5}$$

$$\frac{\partial}{\partial x^1}(\frac{1}{D}\frac{\partial y^2}{\partial x^1}) + \frac{\partial}{\partial x^2}(D\frac{\partial y^2}{\partial x^2}) = 0 \tag{6}$$

The generation procedure is as follows. First, the desired grid distribution is specified at the boundaries and those resulting grid points at the boundaries will be kept fixed. Initial y^1 and y^2 values are now guessed, usually by interpolating between boundary values. D for each mesh is computed and is smoothed using a five point smoother. The system of eqns. 5 and 6 is now solved to obtain new y^1 and y^2 by a solver,eg. Tridaigonal Matrix Algorithm(TDMA).

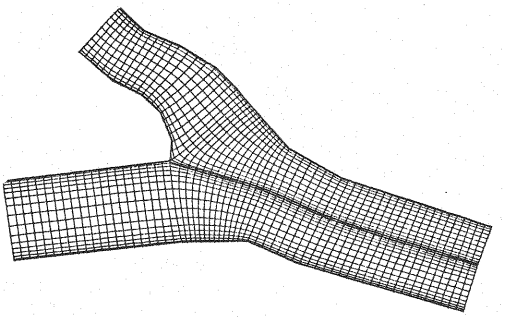

Fig. 1 Part of generated grid
(Tone - Watarase river confluence)

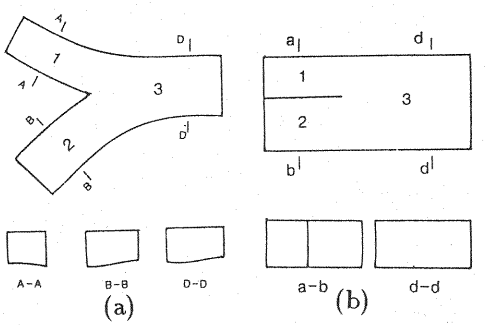

Fig. 2 (a) Physical domain
(b) Computational domain

Several sweeps of TDMA is made with updated D each time and the number of sweeps is decided after viewing the grid on graphics. The above procedure transforms uniform square meshes in the transformed plane to smooth and nearly orthogonal curvilinear meshes in the physical plane. Part of two-dimensional grid generated following this method, for Tonegawa-Watarasegawa river confluence, is shown in Fig. 1. The extension to the third dimension is now done by the interpolation upon the condition that bed level variation is smooth and not large.

The transformation relations such as metric tensor, the Christoffel symbols are computed numerically in order to transfer the three-dimensional confluence region with curvilinear meshes, the physical domain shown in Fig.2(a), to a parallelepiped with square meshes, the computational domain shown in Fig.2(b).

MATHEMATICAL MODEL

Governing equations and turbulence model

The equations governing the motion of steady, incompressible, three-dimensional turbulent flows are continuity equation and time-averaged Navier Stokes equations, and they can be written in the following tensor form using contravariant velocity components.

$$U^i{}_{;i} = 0 \tag{7}$$

$$(U^iU^j)_{;j} = f^i - \frac{1}{\rho}p^{,i} + (\nu U^{i}{}_{;}{}^{j} - \overline{u^iu^j})_{;j} \tag{8}$$

where U^i = contravariant component of mean velocity; u^i = contravariant component of turbulent velocity; p = piezometric pressure; ν = kinematic viscosity; a semicolon = covariant differentiation; comma = differentiation; and overbar = time averaging process.

Eddy viscosity concept and the standard $k-\epsilon$ turbulence model are used to compute the turbulent stresses. The related equations can be written in the following generalized form.

Eddy viscosity concept,

$$-\overline{u^iu^j} = \nu_t(U^{i}{}_{;}{}^{j} + U^{j}{}_{;}{}^{i}) - \frac{2}{3}g^{ij}k \tag{9}$$

$k-\epsilon$ turbulence model,

$$(kU^j)_{;j} = (\frac{\nu_t}{\sigma_k}k^{,j})_{;j} + \nu_t(U_i{}^{;j} + U^j{}_{;i})U^i{}_{;j} - \epsilon \tag{10}$$

$$(\epsilon U^j)_{;j} = (\frac{\nu_t}{\sigma_\epsilon}\epsilon^{,j})_{;j} + c_1\frac{\epsilon}{k}\nu_t(U_i{}^{;j} + U^j{}_{;i})U^i{}_{;j} - c_2\frac{\epsilon^2}{k} \tag{11}$$

$$\nu_t = c_\mu \frac{k^2}{\epsilon} \tag{12}$$

where k = turbulent kinetic energy; ϵ = the rate of energy dissipation; ν_t = eddy viscosity; and u_i = covariant component of mean velocity. The constants appear in the $k-\epsilon$ turbulence model have the standard values as given by Rodi(19).

Boundary conditions

Boundary conditions must be specified on the all surfaces of the computational domain. The fully developed flow conditions, computed by another model, are input as inflow in both channels. At the outflow plane, zero gradients in the streamwise direction are imposed to all variables except pressure. The wall function approach given by Launder and Spalding(10) is used to treat the bottom and side walls. Accordingly, the resultant velocity component parallel to the wall V_p at the first grid point at a distance y_p from the wall is related to resultant friction velocity u_* as

$$\frac{V_p}{u_*} = \frac{1}{\kappa} ln(Ey^+) \tag{13}$$

where κ = the von Karman constant(=0.42); y^+ = non dimensional wall distance $u_* y_p/\nu$ and $(30 \leq y^+ \leq 100)$; and E = roughness parameter. And, $E = 9$ is taken here considering the surfaces are smooth. In the wall region, local equilibrium prevails and turbulent kinetic energy and energy dissipation rate at the first grid point are specified as

$$k = \frac{u_*}{\sqrt{c_\mu}} \tag{14}$$

$$\epsilon = \frac{u_*^3}{\kappa y_p} \tag{15}$$

Also the resultant shear stress parallel to the boundary surface over the region is considered to be the same as the wall shear stess τ_w given by

$$\tau_w = \rho u_*^2 \tag{16}$$

The shear stresses at the boundaries of the computational domain are derived as follows. If the covariant components of the unit normal vector on the surface F where coordinate x^i is constant are given by

$$\begin{aligned} n_l &= \frac{\partial F}{\partial x^l} / |\nabla F| \\ &= \frac{1}{\sqrt{g^{\underline{ii}}}} \delta_i^l \end{aligned} \tag{17}$$

where δ_i^l = the Kronecker delta and no summation in $g^{\underline{ii}}$. Then, the shear stress vector $\vec{T}$ on the surface is given by

$$\begin{aligned} \vec{T} &= \tau^{ij} n_i \vec{g_j} \\ &= \frac{\tau^{ij}}{\sqrt{g^{\underline{ii}}}} \vec{g_j} \end{aligned} \tag{18}$$

where τ^{ij} is the contravariant stress tensor. The shear stress vector $\vec{T}$ on the surface can also be written as a combination of covariant and contravariant physical components as

$$\vec{T} = \frac{\tau^{(ij)}}{\sqrt{g_{\underline{jj}}}} \vec{g_j} + \frac{\tau_{(\underline{ii})}}{\sqrt{g^{\underline{ii}}}} \vec{g^i}, \quad j \neq i \tag{19}$$

Eqns. 18 and 19 are equated and τ^{ij} necessary as boundary condition are obtained in terms of physical components. $\tau^{(ij)}$ are computed from eqns. 13 and 14 and $\tau_{(\underline{ii})}$ is specified as consistent with the $k-\epsilon$ model.

The free surface is treated as a frictionless rigid-lid symmetry plane (see e.g. Leschziner and Rodi(11)) where the vertical velocity component and the normal gradients of other variables are set to zero. This does take into account the surface elevation changes through the pressure gradients along lateral and transverse directions.

Solution procedure

The partial differantial eqns. 7 to 12 are written in the conservative form using tensor identities (Gal-chen(8), Sokolonikoff(20)) and can be arranged to following common form.

$$\frac{\partial}{\partial x^i}\sqrt{g}(\rho U^i\phi - \mu_{eff}g^{\underline{ii}}\frac{\partial\phi}{\partial x^i}) = S_\phi \qquad (20)$$

where $g = det[g_{ij}]$; ϕ takes u, v, w, k, ϵ and the continuity equation comes as a special case when $\phi = 1$ and $S_\phi = 0$. Eqn. 20 is integrated over the respective control volumes on staggered grid system (Patankar(16)) in the computational domain following the partially parabolic procedure of Pratap and Spalding(17). This procedure enables downstream marching solution and but downstream effect is allowed to transfer upstream through the pressure. However, on the other hand it limits the model applicability to confluences with no recirculation.

The pressure correction equation is derived from continuity equation, considering the effect of all three pressure gradients, which appear due to the nonorthogonality of the grids, on the velocity correction terms. The hybrid scheme is employed to evaluate the coefficients in the cross-stream. A procedure similar to the SIMPLE algorithm is then used to obtain the converge solution by making sweeps from upstream to downstream.

MODEL PREDICTIONS AND DISCUSSION

The mathematical model introduced above was first applied to simple problems to verify its performances. That includes the experimentally studied cases of developing duct flow (Melling and Whitelaw(13)) and parallel flow confluence flow (Koike(9)). The comparisons in the latter case is summerized here. The layout of their experiment carried out in a flume of 15m long with a partition wall of 1mm thick and 7.7m long(Fig. 3). The water depth d was 10cm and the measurements were done by hot-film anemometer at $h/d = 0.8$, where h is the distance measured from the bottom of the flume.

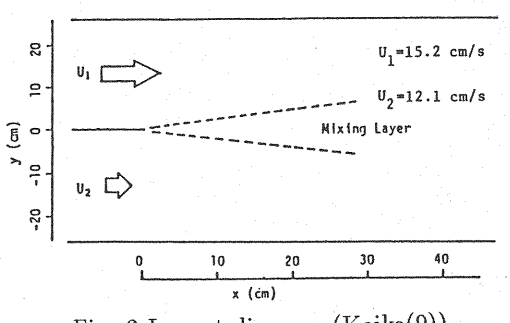

Fig. 3 Layout diagram (Koike(9))

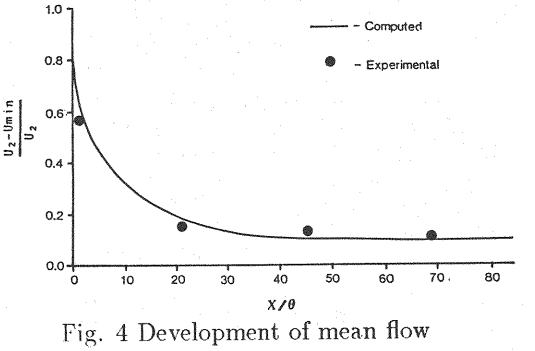

Fig. 4 Development of mean flow in the mixing layer

Computation was done for the case of discharge ratio of 0.8 shown in Fig.3, using a 50x40x9 grid over the length of -100cm $< x <$ 700cm. X and Y are measured as indicated in Fig.3. Grid lines were concentrated at the mixing region and near wall region and the thickness of the partition wall was neglected. Fig.4 depicts the development of the mean flow in the mixing layer and Fig. 5 shows the comparison of longitudinal velocity profiles at different sections in the mixing region. Although this turbulent mixing layer is dominated by the periodic eddies, the above depictions clarify that the model predicts the mean flow quantities to a reasonable accuracy.

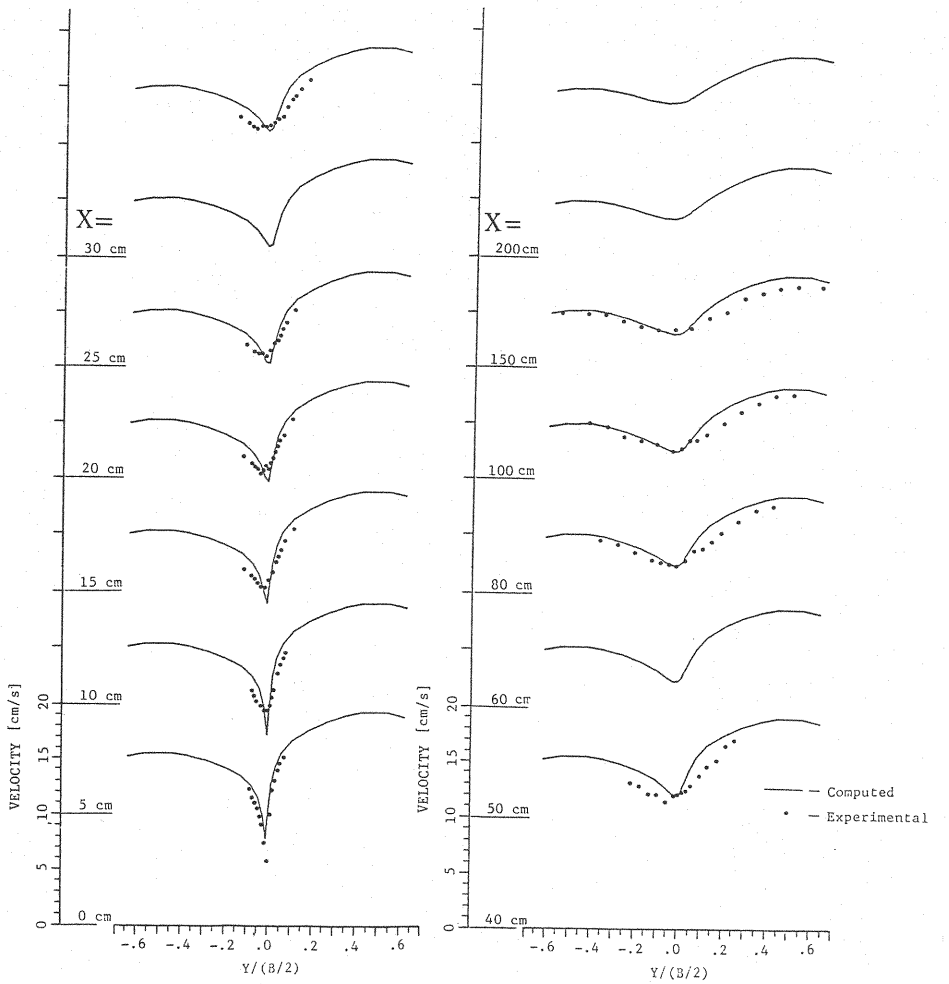

Fig. 5 Longitudinal mean velocity profiles in the mixing layer at $h/d = 0.8$

At the next step, the model was employed to predict the three-dimensional flow in the confluence of 60 degrees, having rectangular cross sections and a training levee studied experimentally by Tada(21). The configuration of the confluence is illustrated in Fig.6. The side walls of the channels were nominally smooth. The discharge in the main channel was 1.646 l/s and that of the branch was 1.366 l/s. The downstream controll and the upstream feeders of the channels were located at 6m and 3m from the confluence respectively, and thus their effect on the confluence was neglegible.

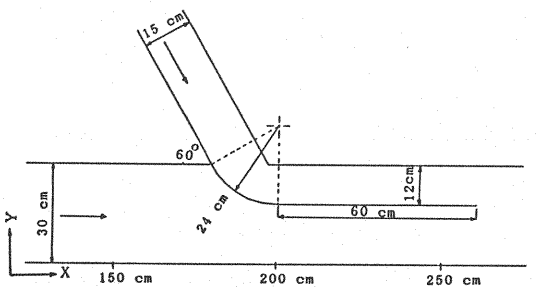

Fig. 6 Layout diagram (Tada(21))

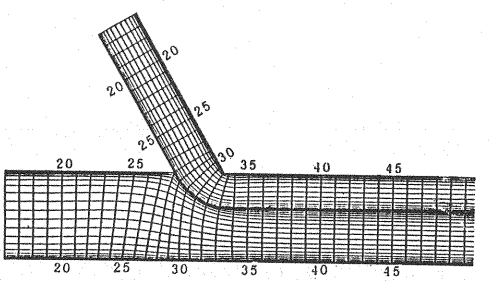

Fig. 7 Part of grid and sections

A total length of 450cm while 300cm being after the confluence was considered in the flow computation. Part of curvilinear grid of 66x36x8 generated is shown in Fig.7. The computation required 35min. in M680 system of Univ. of Tokyo.

The comparison of the longitudinal components of the velocity vector drawn in streamwise vertical sections is shown in Fig.8, where h is the depthwise coordinate measured from the bottom and X,Y are measured as indicated in Fig.6. The velocity scales are the same for each curve and the 9 curves given in each figure corresponding to the different values of X progressing downstream as given in the figure caption. As can be seen from Fig.8, the prediction agrees quite well with the measurements, except in a narrow region where very low velocities appear near the downstream corner of the geometric junction (e.g. Fig.8(a)). However, this is the location where the pressure and velocity gradients are high, streamlines are much curved and deviate more from the grid lines; thus such descrepancy could be possible as the model employs hybrid scheme and the standard $k-\epsilon$ model. Also, a small overestimation of the velocities is shown in general throughout this developing flow region. This discrepancy rises to ensure the continuity of the flow, because the actual water depths in this region are greater than the imposed constant water depth corresponding to the actual downstream water depth by a maximum of about 10symmetry plane boundary condition imposed at the top surface, but the water depths are computed from the pressure gradients (see e.g. Demuren and Rodi(5), Tamai and Ueda(22)). The comparison of water depth variation with experimentally obtained values shows satisfactory agreement as depicted in Fig. 9 . Fig.10 shows the piezometric pressure contours which correspond to the variation of water surface level in the region.

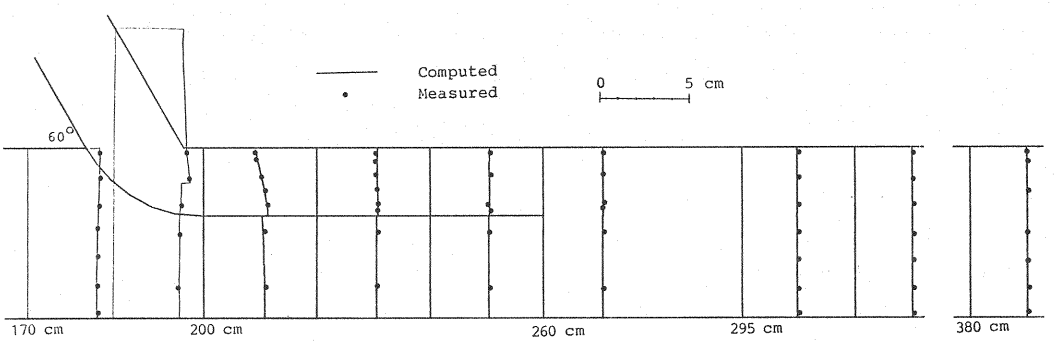

Fig. 9 Flow depth variation

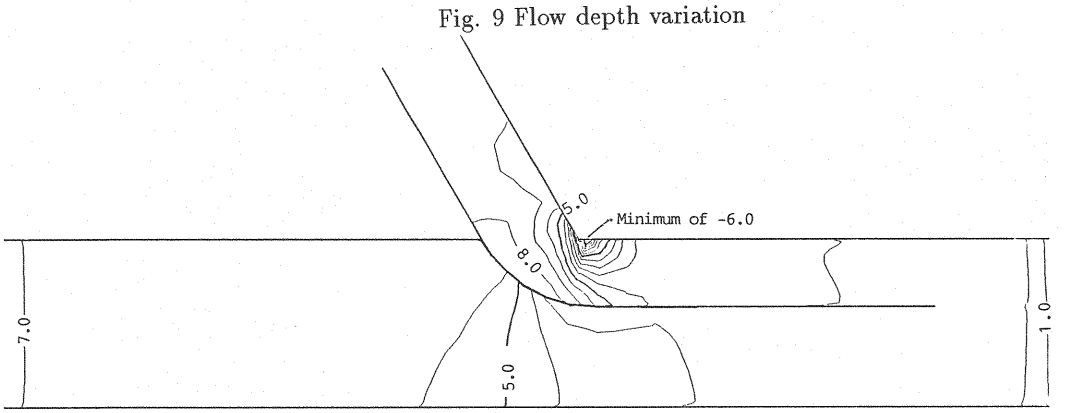

Fig. 10 Piezometric pressure contours (contour interval of $1mm$)

According to Figs. 9 and 10, the superelevation of the both flow channels towards the levee is prominent. If the levee is absent, strong mixing will occur between two flows and thus the superelevation in the branch channel which is substantial at the present case can be expected to be smaller, but on the other hand the superelevation towards the right bank at the main channel can be expected to be larger(see e.g. Tamai and Ueda(22)). The levee also prevents the jet-like intrusion of the flow of branch channel which causes considerable backwater effect in the main channel, specially at large discharge ratios. Thus, the training levee reduces the flood risk.

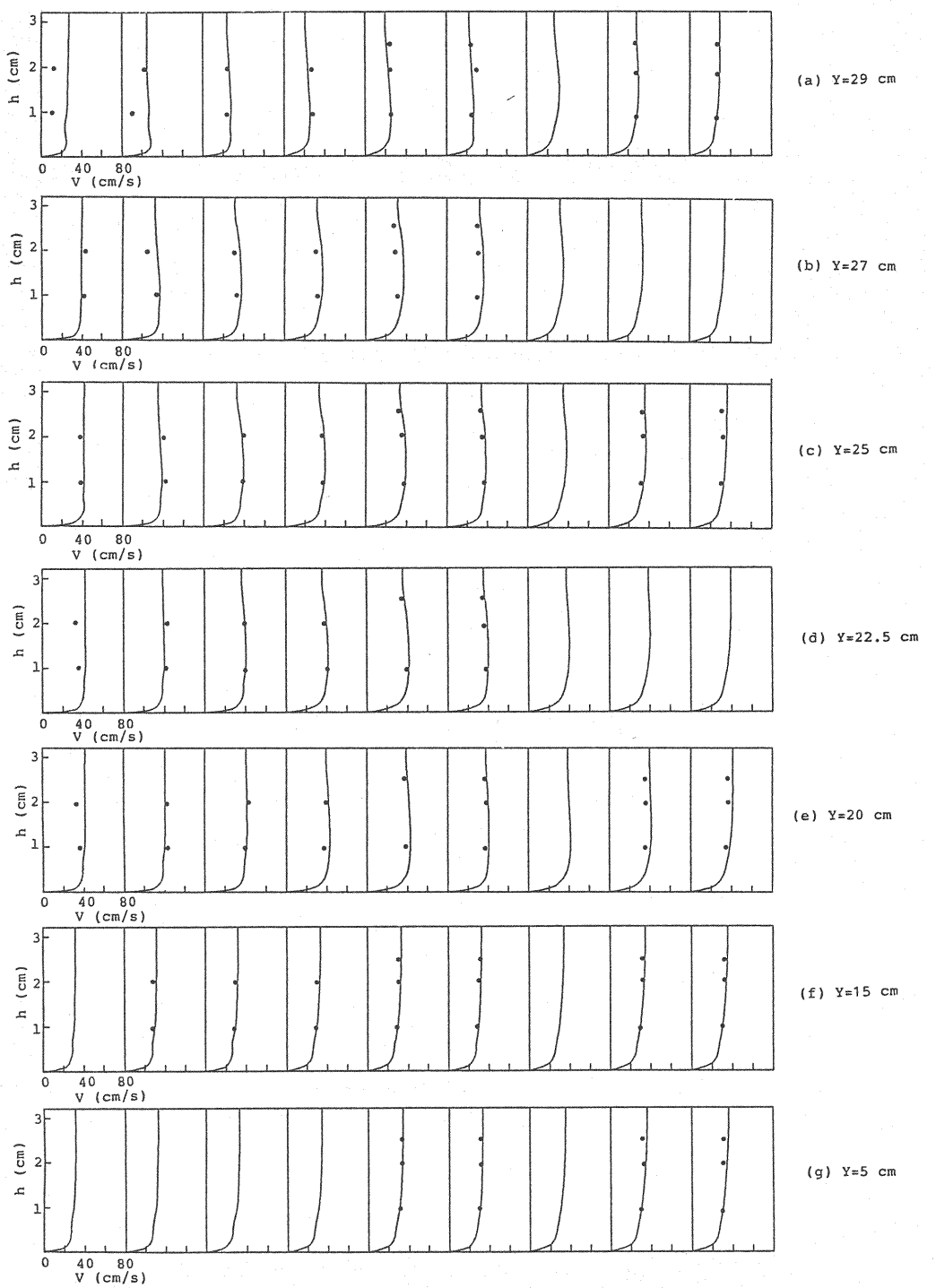

Fig. 8 Longitudinal velocity profiles at
X = 200,215,235,265,270,280,325,380 and 480 cm respectively

In the absence of the training levee, a recirculation zone would appear and its dimensions can be estimated according to discharge ratio, confluence angle, Froude numbers and momentum ratio (see e.g. Best and Reid(3)). However, as the experimental results in Fig.(8) depict, the training levee has eliminated the recirculation zone and which in turn has enable the model to predict the associated flow pattern (Figs. 11,12,13). Fig. 11 shows the velocity vectors in plane sections at near bottom and near surface. Accordingly, the whole channel width is effectively utilized by the flow and the velocity of the flow is reduced.

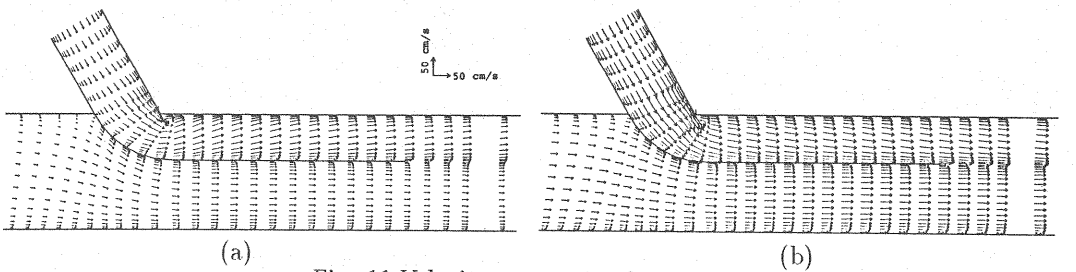

Fig 11. Velocity vectors in plane sections
(a) Near bed (b) Near surface

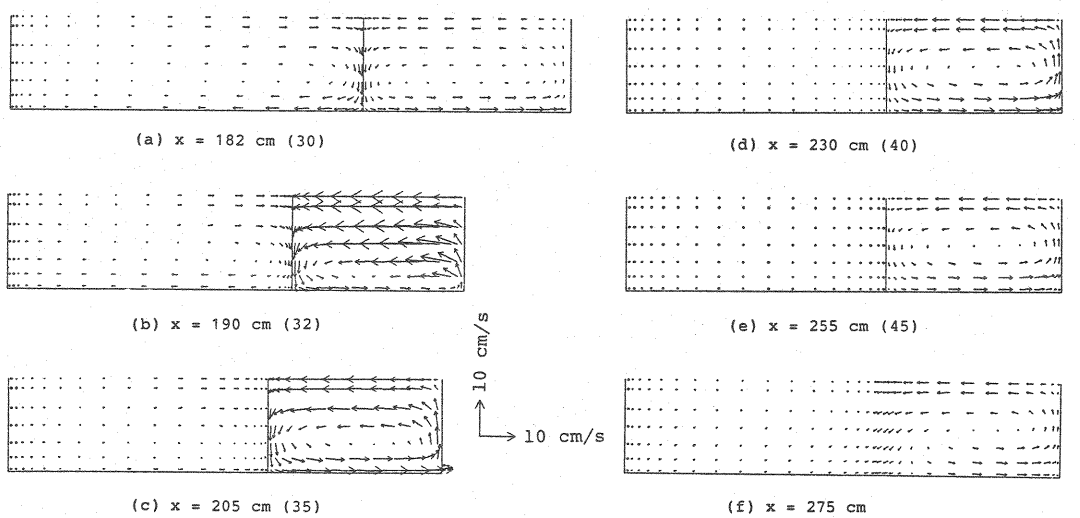

Fig.12 Secondary flow

Fig. 12 shows the secondary flow vectors in lateral sections: the sections are as shown in Fig.6 and Fig.7. The spiral motions which counter rotate appear in two channels at the bothside of the levee. These two vortexes appear for the reason of continuity as the fluid particles follow a curved path. The vortex in the branch channel which is comparatively large is shown not to have decayed completely before two flows join at the end of the levee. The secondary flow in the branch channel has the maximum value of about 30% of the average branch channel velocity at sections closer to the left bank corner of the confluence. The presence of training levee has blocked strong mixing of the flows at the junction and thus reduced the secondary flow in the main channel that would appear otherwise (see e.g. Tamai and Ueda(22)). On the other hand it has blocked momentum transfer thus resulting a slow decaying strong vortex in the branch channel. The levee has made mixing of two flows gradual as flows depart the levee and thus it has reduced the superelevation in the mixing region which appears in confluence without a training levee (see e.g. Tamai and Ueda(22)). Fig. 13 shows the velocity isovels of the sections. The strong secondary motion has caused isovels to skew towards the concave bank and the maximum velocity to appear below the water surface. Fig. 14 shows the computed bed-shear stress contours. The shear stress distribution which follows that of bottom velocity, shows the maximum stress in the branch channel closer to the downstream corner of the confluence and the maximum in the main channel closer to the levee. The maximum values are about 4 times the maximums at the upstreams of the respective channels.

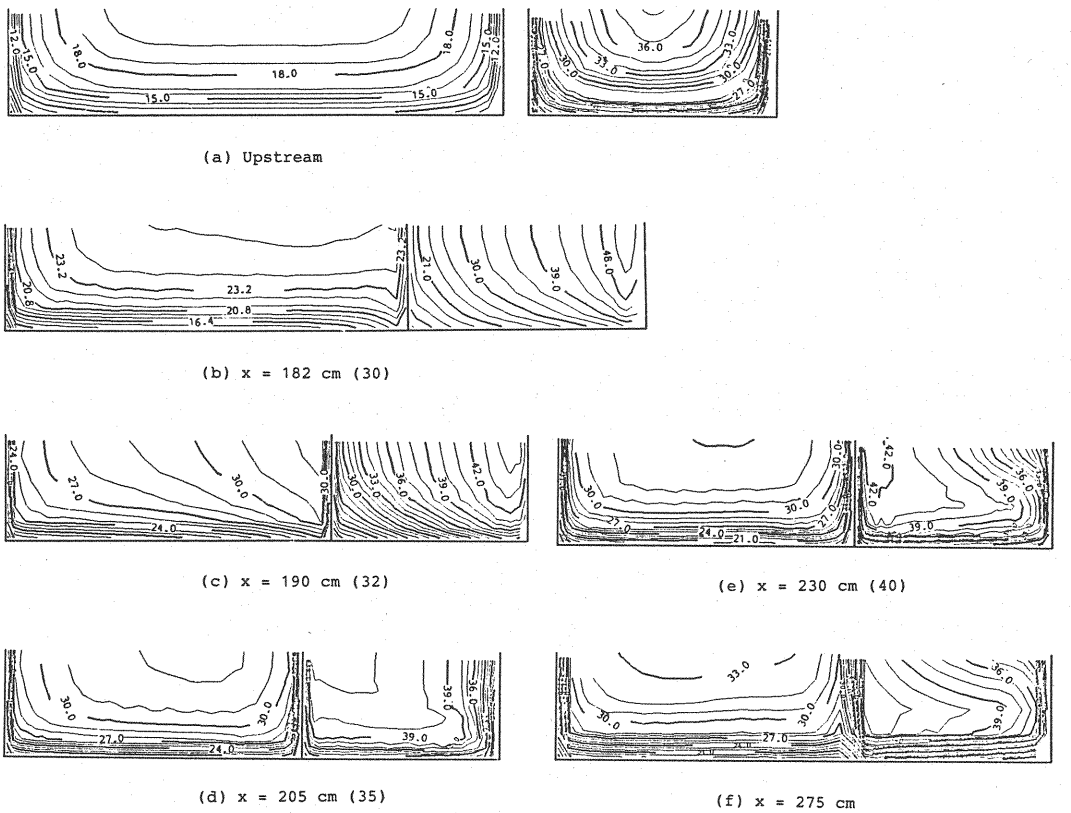

Fig.13 Velocity isovels

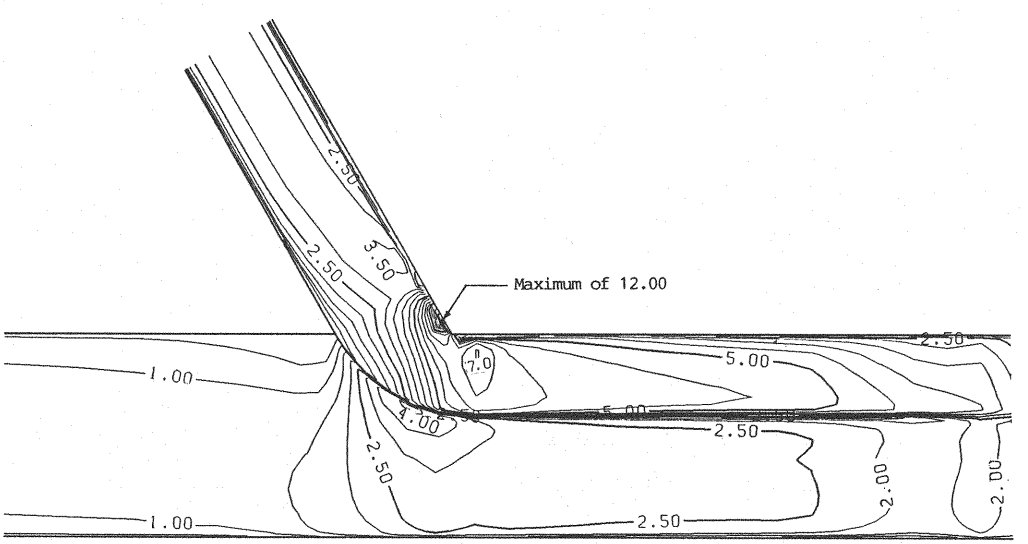

Fig. 14 Bed-shear stress contours (contour interval of $0.5 dyne/cm^2$)

CONCLUDING REMARKS

a) A three-dimensional mathematical model based on the standard $k-\epsilon$ turbulence model has been presented for the confluences with no recirculation zone. The agreement of the computed results with experimental results is generally good. However, three-dimensional elliptic flow model is necessary to predict the flow in a general confuence in detail.

b) The grid generation method adopted is simple and can be used to tackle an arbitrary confluence and is flexible in spacing of grids.

c) The performance of a levee has been demonstrated. The levee prevents strong mixing and facilitates two streams to mix gradually. Thereby superelevation in the junction and the strong secondary flow in the main stream are considerably reduced. The levee prevents large back water effect in the main stream at large discharge ratio. It also increases the effective channel width by eliminating the recirculation zone.

AKNOWLEDGEMENTS

The authors are grateful to Mr.H.Tada, Osaka College of Technology and Dr.I.Nezu, Kyoto University for providing experimental data and also to Dr.Y.Kawahara at the department and to Dr.Evegini Sullinen, Riga Polytechnic Institute, USSR for their useful comments. The study was partly supported by the Grant in Aid of the Ministry of Education, Science and Culture of Japan in the category of Effective Counter Measures for Natural Disasters (Principal investigator, Prof. Kishi, Hokkaido University).

REFERENCES

1. Ashmore, P. and G. Parker : Confluence scour in coarse braided streams, J. of Water Resources Research, Vol.19, No.2, pp.392-402, 1983.
2. Best, J.L. : Sediment transport and bed morphology at river channel confluences, J. of Sedimentalogy, Vol.35, pp.487-498, 1988.
3. Best, J.L. and I. Reid : Separation zone at open-channel flow junctions, J. of Hydr. Engrg., ASCE, Vol.110, No.11, pp.1588- 1594, 1984.
4. Chen,C.J., K.M. Obasih and T.S. Wang : Numerical generation of nearly orthogonal boundary-fitted coordinate system, Numerical Grid Generation in Computational Fluid Mechanics, First ed., Pineridge Press, Swansea, U.K., 1988.
5. Demuren, A.O. and W. Rodi : Calculation of flow and pollutant dispersion in meandering channels, J. of Fluid Mech., Vol.172, pp.63-92, 1986.
6. Fujita, I. and S. Komura :Application of the free stream line theory to the flow in a river confluence, 5th congress, APD-IAHR, pp.103-120, 1986.
7. Fujita, I. and S. Komura : Visualization of the flow at a river confluence, Proc. of the 3rd Int. Symp. on Refined flow Modelling and Turbulence Measurements (Tokyo, Japan), pp.611-618, July 1988.
8. Gal-chen, T. and C.J.S. Richards : On the use of a coordinate transformation for the solution of the Navier-Stokes equation, J. of Comp. Phys., Vol.17, pp.209-228, 1975.
9. Koike, A. : Organized vortex in a river confluence, M.E.thesis, Kyoto univ., 1986, (in Japanese).
10. Launder, B.E. and D.B. Spalding : The numerical computations of turbulent flows, Comp. Methods in App. Mech. and Engrg., Vol.3, pp.269-289, 1974.
11. Leschziner, M.A. and W. Rodi : Calculation of strongly curved open channel flow, J. of Hyd. Div., ASCE, Vol.104, Hy10, pp.1297- 1314,1979.
12. Mastin, C.W. and J.F. Thompson : Quasiconformal mappings and grid generation, SIAM J. of Sci. Stat. Comput., Vol.5, No.2, pp.305-310, 1984.
13. Melling, a. and J.H. Whitelaw : Turbulent flow in a rectangular duct, J. of Fluid Mech., Vol.78, pp.289-315, 1976.
14. Modi, P.N., P.D. Ariel and M.M. Dandekar : Conformal mapping for channel junction flow, J. of Hydr. Div., ASCE, Vol.107, HY12, pp.1713-1733, 1981.
15. Mosely, M. P. : An experimental study of channel confluences, J. of Geology, Vol.94, pp.535-562, 1976.
16. Patankar, S. V. : Numerical Heat Transfer and Fluid Flow, Hemisphere, N.Y., 1980.
17. Pratap, V.S. and D.B. Spalding : Fluid flow and heat transfe r in three-dimensional duct flow, Int. J. of Heat Transfer, Vol.109, pp.1183-1188, 1976.
18. Ramamurthy, A.S., L.B. Carballada and D.M. Tran : Combining open channel flow at right angled junctions, J. of Hydr. Engrg., ASCE, Vol.114, No.12, pp.1449-1459, 1988.
19. Rodi, W. : Turbulence Models and their Applications in Hydraulics, Monograph, IAHR, Delft, The Netherlands, 1980.
20. Sokolonikoff, I.S : Tensor Analysis, John Willy Inc., N.Y., 1964.
21. Tada, H. : Experimental report, Osaka College of Technology, 1987, (in Japanese).

22. Tamai, N. and S. Ueda : Prediction of flow behaviour at river confluences by the $k-\epsilon$ model, Proc. of the 31st Japanese Conf. on Hydraulics, pp.437-442, 1987, (in Japanese).
23. Taylor, E.H. : Flow characteristics at rectangular open channel junctions, Trans., ASCE, Paper No.2223, 893-912, 1944.
24. Thompson, J. F. and Z. V. A. Warsi : Boundary-fitted coordinate systems for numerical solution of partial-differential equations- A review, J. fo Comp. Physics, 47, pp. 1-108, 1982.
25. Webber N.B. and C.A. Greated : An investigation of flow behaviour at junction of rectangular channels, Proc. of Inst. Civil Engrs., Vol.34, pp.321-334, 1966.

APPENDIX-NOTATION

The following symbols are used in this paper:

B	= channel width;
c_μ, c_1, c_2	= constants in the $k-\epsilon$ model;
D	= grid aspect ratio;
E	= roughness parameter;
$\vec{g_r}$	= base vectors in curvilinear coordinate system;
g_{rs}	= metric tensor;
g^{rs}	= reciprocal metric tensor;
g	= determinant of the metric tensor;
d	= water depth;
h	= elevation measured from the channel bottom;
$\vec{i}$	= unit vectors in Cartesian coordinate system;
k	= kinetic energy of the fluctuation motion of the flow;
n_i	= covariant components of a unit normal to a surface;
p	= piezometric pressure;
S_ϕ	= source term in descretized equation;
$\vec{T}$	= shear stress vector on a surface;
U^i, U_i	= contravariant and covariant velocity components of mean velocity;
u^i, u_i	= contravariant and covariant velocity components of fluctuating velocity;
u_*	= local shear velocity;
V_p	= velocity component tangential to the surface;
x^i	= coordinate axes in a general curvilinear coordinates system: i=1,2,3 are in the directions of streamwise, lateral and vertical respectively;
y^i	= coordinate axes in Cartesian coordinate system (correspondence is similar to y above);
y_p	= local distance from the wall;
y^+	= nondimensional wall distance;
comma	= differentiation;
overbar	= time averaging process;
semicolon	= covariant differentiation;
δ^i_j	= the Kronecker delta;
ϵ	= rate of energy dissipation;
κ	= Von Karmann constant;
μ_{eff}	= effective viscosity;
ν_t	= eddy viscosity;
ρ	= density of water;
$\sigma_k, \sigma_\epsilon$	= constants in the $k-\epsilon$ model;
τ^w	= magnitude of the wall shear stress;
τ^{ij}	= contravariant components of the stress tenso;r and
$\tau^{(ij)}, \tau_{(ij)}$	= physical components of corresponding contravariant and covariant components.